Journal of Radioanalytical and Nuclear Chemistry (2025) 334:7035–7049
https://doi.org/10.1007/s10967-025-10361-2

Prompt gamma rays of neodymium from the (n,n´γ)- reaction with fission neutrons

Niklas Ophoven[1] · Eric Mauerhofer[1] · Zeljko Ilic[1,2] · Christian Stieghorst[3] · Zsolt Révay[3] · Iaroslav Meleshenkovskii[1] · Tsitohaina H. Randriamalala[1]

Received: 26 May 2025 / Accepted: 14 August 2025 / Published online: 1 September 2025

Abstract
Prompt gamma-ray emission generated by the (n,n′γ) reaction during irradiation of a $NdCl_3$ sample with fission neutrons was studied with the instrument fast neutron-induced gamma-ray spectrometry (FaNGaS) at Heinz Maier–Leibnitz Zentrum (MLZ). We present relative intensities and production cross sections for 111 identified gamma lines of neodymium. The results participate to extend and enhance literature on nuclear data. The detection limit of neodymium is 2.1 mg for a measuring time of 12 h.

Keywords Inelastic scattering · Neodymium · Fast neutron · Chlorine · Cross section · Gamma ray

Introduction

The measurement of prompt gammas released from various nuclear reactions during the irradiation of samples or items with a beam of free neutrons is a well-established method for nondestructive chemical analysis. While prompt gamma neutron activation analysis (PGNAA) using cold and thermal neutrons [1] is mostly limited to small and thin samples, prompt gamma analysis based on inelastic neutron scattering (PGAINS) offers the possibility to investigate large and thick samples [2–4] owing to the higher penetration depth of utilized fast neutrons. PGAINS is promising for the nondestructive characterization of high-performance permanent magnets like NdFeB, SmCo, AlNiCo, which recycling is of prime importance as they contain neodymium, praseodymium, dysprosium, terbium, boron, samarium, nickel and cobalt. Indeed, these elements are defined as critical raw materials (CRMs) by the European Union due to their economic and technological importance and their delivery risks [5, 6]. Their recovery from permanent magnets is one particular action of the European Critical Raw Material Act (§ 57) [7] to ensure a resilient supply. A prerequisite for efficient recycling is the sorting of the different types of magnets through the determination of their elemental composition. Recently, it was shown with numerical simulations that PGAINS in conjunction with a compact accelerator-based neutron source generating a high fast neutron flux could be suitable for a rapid chemical analysis of neodymium iron boron (NdFeB) permanent magnets in view of their industrial recycling [8]. However, reliable and accurate quantification necessitates knowledge on the cross sections for production of prompt gamma rays induced by inelastic scattering of fast neutrons i.e. (n,n´γ) reactions or by other reactions like (n,p) and (n,α). In previous works, the production cross-sections of gamma rays emitted by interaction of fission neutrons (average energy of 2.2 MeV) on 19 elements (C, O, Na, Al, Si, S, Cl, K, Ca, Ti, Fe, Ni, Cu, Zr, In, La, Ce, Pr, Tb) were measured [9–17]. This was achieved by using the FaNGaS (Fast Neutron induced Gamma-ray Spectrometry) instrument operated at MLZ (Heinz-Maier-Leibnitz Zentrum) [9, 12, 18].

In this work, relative intensities and production cross sections of neodymium prompt gamma lines produced by inelastic scattering of fission neutrons on a neodymium(III) chloride ($NdCl_3$) sample are presented and discussed with regard to available literature data. In

✉ Eric Mauerhofer
e.mauerhofer@fz-juelich.de

[1] Jülich Centre for Neutron Science, Forschungszentrum Jülich GmbH, 52425 Jülich, Germany

[2] Lehrstuhl Für Experimentalphysik IVc, RWTH Aachen University, 52056 Aachen, Germany

[3] Heinz Maier-Leibnitz Zentrum (MLZ), Technische Universität München, Lichtenbergstraße 1, 85748 Garching, Germany

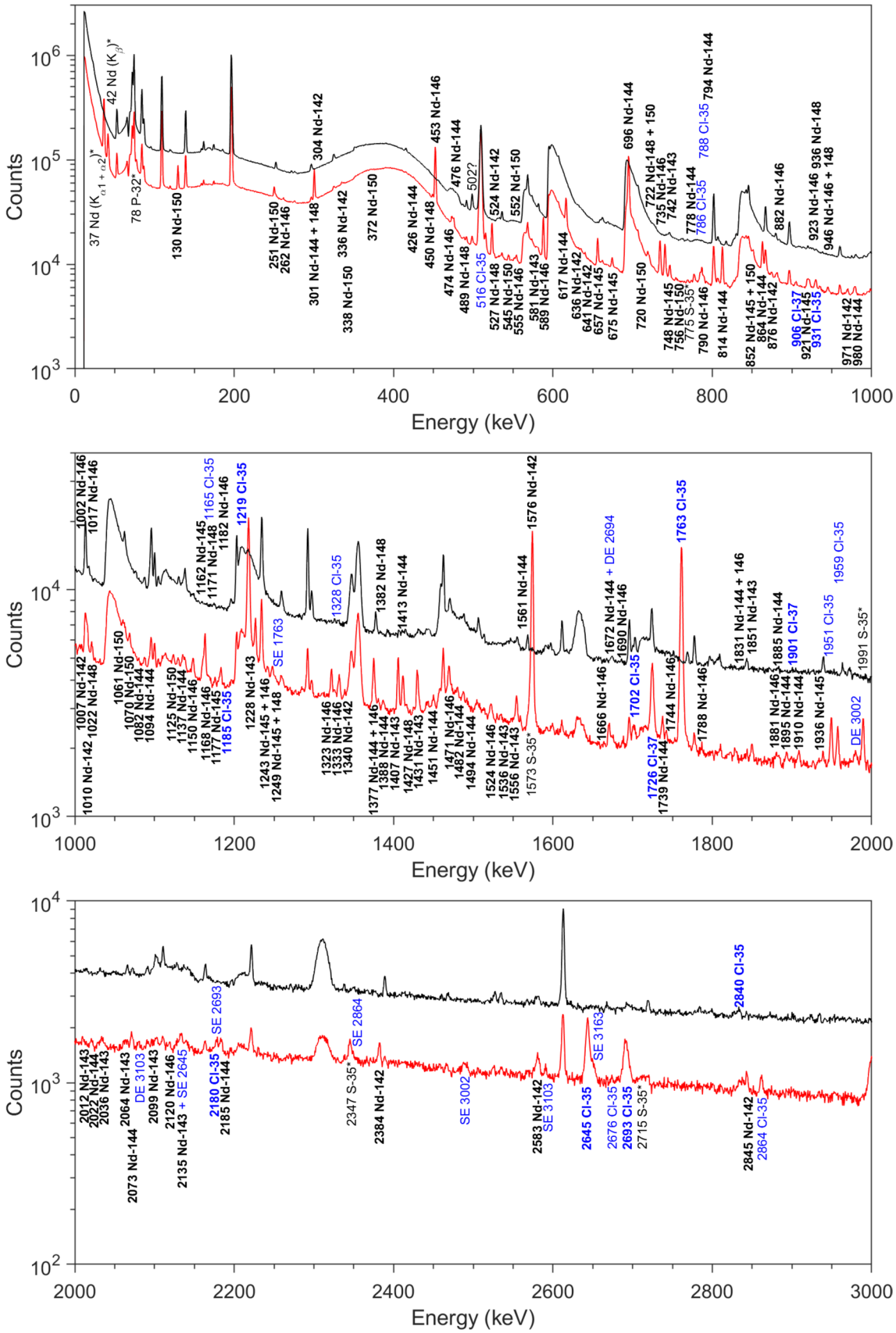
Counts
Energy (keV)
37 Nd (K$_{\alpha1+\alpha2}$)*
42 Nd (K$_\beta$)*
78 P-32*
130 Nd-150
251 Nd-150
262 Nd-146
301 Nd-144 + 148
304 Nd-142
336 Nd-142
338 Nd-150
372 Nd-150
426 Nd-144
450 Nd-148
453 Nd-146
474 Nd-146
476 Nd-144
489 Nd-148
502?
516 Cl-35
524 Nd-142
527 Nd-148
545 Nd-150
552 Nd-150
555 Nd-146
581 Nd-143
589 Nd-146
617 Nd-144
636 Nd-142
641 Nd-142
657 Nd-145
675 Nd-145
696 Nd-144
720 Nd-150
722 Nd-146
735 Nd-148 + 150
742 Nd-143
748 Nd-145
756 Nd-150
775 S-35*
778 Nd-144
786 Cl-35
788 Cl-35
790 Nd-146
794 Nd-144
814 Nd-144
852 Nd-145 + 150
864 Nd-144
876 Nd-142
882 Nd-146
906 Cl-37
921 Nd-145
923 Nd-146
931 Cl-35
936 Nd-148
946 Nd-146 + 148
971 Nd-142
980 Nd-144
1002 Nd-146
1007 Nd-142
1010 Nd-142
1017 Nd-146
1022 Nd-148
1061 Nd-150
1070 Nd-150
1082 Nd-144
1094 Nd-144
1125 Nd-150
1137 Nd-144
1150 Nd-146
1162 Nd-145
1165 Cl-35
1168 Nd-146
1171 Nd-148
1177 Nd-145
1182 Nd-146
1185 Cl-35
1219 Cl-35
1228 Nd-143
1243 Nd-145 + 146
1249 Nd-145 + 148
SE 1763
1323 Nd-146
1328 Cl-35
1333 Nd-146
1340 Nd-142
1377 Nd-144 + 146
1382 Nd-148
1388 Nd-144
1407 Nd-143
1413 Nd-144
1427 Nd-148
1431 Nd-143
1451 Nd-144
1471 Nd-146
1482 Nd-144
1494 Nd-144
1524 Nd-146
1536 Nd-143
1556 Nd-143
1561 Nd-144
1573 S-35*
1576 Nd-142
1666 Nd-146
1672 Nd-144 + DE 2694
1690 Nd-146
1702 Cl-35
1726 Cl-37
1739 Nd-144
1744 Nd-146
1763 Cl-35
1788 Nd-146
1831 Nd-144 + 146
1851 Nd-143
1881 Nd-146
1885 Nd-144
1895 Nd-144
1901 Cl-37
1910 Nd-144
1936 Nd-145
1951 Cl-35
1959 Cl-35
1991 S-35*
DE 3002
2012 Nd-143
2022 Nd-144
2036 Nd-143
2064 Nd-143
DE 3103
2073 Nd-144
2099 Nd-143
2120 Nd-146
2135 Nd-143 + SE 2645
2180 Cl-35
SE 2693
2185 Nd-144
2347 S-35*
SE 2864
2384 Nd-142
SE 3002
2583 Nd-142
SE 3103
2645 Cl-35
SE 3163
2676 Cl-35
2693 Cl-35
2715 S-35*
2840 Cl-35
2845 Nd-142
2864 Cl-35

◂**Fig. 1** Measured gamma-ray spectra in the energy range from 0 to 3000 keV. The spectrum of the NdCl3 sample (red) was obtained during 8886 s counting live time and the spectrum of the beam background (black) during 51,506 s. Prompt gamma rays that are written in black with an asterisk belong to either (n,pγ) reactions (S-35) and (n,αγ) reactions (P-32) on Cl-35 or represent X-rays from neodymium. Prompt gamma rays marked in black and bold are issued from (n,n′γ) inelastic scattering of fast neutrons on neodymium. Gamma rays written in bold blue are induced by inelastic scattering reactions on chlorine. Radiative capture gamma rays from Cl-35 are marked with light blue. Single and double escape peaks are indicated by the abbreviations SE and DE, respectively. Our former publications [9, 18] provide information on the origin of relevant background lines

addition, cross sections measured for chlorine lines are compared with the values obtained in [13]. Furthermore, we give the elemental detection limit for neodymium.

Experimental

Prompt gamma radiation was generated upon interactions of fission neutrons with a $NdCl_3$ powder sample (mass: 1.87 g, Nd: 1.07 g, Cl: 0.79 g) and detected using the FaNGaS instrument presented in [12]. The powder was contained and irradiated in a small bag of PTFE (polytetrafluoroethylene). The sample thickness was estimated to be 3 mm. The sample was tilted by an angle of 45° with respect to the incident beam direction. The thermal (10^{-10} MeV < E_n < 1.4×10^{-7} MeV), epithermal (1.4×10^{-7} MeV < E_n < 0.06 MeV) and fast (0.06 MeV < E_n < 20 MeV) neutron fluxes at sample position were $(3.2 \pm 1.3) \times 10^3$ cm^{-2} s^{-1}, $(2.9 \pm 0.8) \times 10^6$ cm^{-2} s^{-1} and $(1.13 \pm 0.04) \times 10^8$ cm^{-2} s^{-1} [14], respectively. The neutron energy spectrum is given in the supplementary materials of [16]. The sample was irradiated for 3.1 h and counted (live time) for 2.5 h. The distance between sample and the HPGe-detector of FaNGaS was 67 cm. The gamma rays were measured at an angle of 90° relative to the neutron beam axis. The recorded spectra are shown in Figs. 1 and 2. They were analyzed using the HYPERMET-PC software [19]. Gamma rays generated from (n,n´γ) reactions were identified using the NuDat 3.0 database [20] as well as related nuclear data given in [21–30]. Neutron capture lines were identified with the PGNAA database, i.e. refs. [31] and [32].

The count rate of background lines was found to be increased by a mean factor of 1.68 ± 0.16 due to the scattering of a certain fraction of the neutrons from the sample in the direction of the HPGe-detector. This factor was used to correct interferences from background lines. Interferences arising from single and escape lines were corrected with the correction curves and procedure given in [13].

Data analysis

The intensities and the production cross sections of the prompt gamma lines were calculated and compared with the data determined in [33] using the same method as described in [16]. The factor $f_{E\gamma}$ for gamma-ray self-absorption was calculated by means of relation (2) given in [16] with a sample effective thickness of 0.42 cm and a sample density of 4.13 g cm^{-3}. The values of the mass attenuation coefficients were taken from the NIST (National Institute of Standards and Technology) photon cross sections database XCOM [34, 35], including coherent scattering. The dependence of $f_{E\gamma}$ on the gamma-ray energy E_γ is depicted in Fig. 3. The relation between the determined intensities (I_R) and the intensities (I_{RD}) given in [33] was analyzed with the following semi-empirical function:

$$I_R = a \bullet \left(I_{RD}\right)^b \tag{1}$$

with a and b the coefficients returned by the fit of the data. In addition, the agreement between the two sets of data was deduced from the distribution of the residuals in unit of standard deviation [σ], calculated, as:

$$R = \frac{I_R - I_{RD}}{\sqrt{\left(s_{I_R}\right)^2 + \left(s_{I_{RD}}\right)^2}} \tag{2}$$

where s is the absolute uncertainty of the intensity.

Interferences of gamma lines induced by radiative neutron capture reactions in the isotopes ^{35}Cl, ^{142}Nd, ^{143}Nd and ^{145}Nd were identified. For their corrections, effective cross sections $<\sigma>$ were calculated by convoluting the (n,γ)-reactions cross sections of the ENDF/B-VIII.0 library [36] with the neutron energy spectrum using the NJOY Nuclear Data Processing System (Version 2016) [37, 38]. The effective cross sections are given in Table 1. Because of large uncertainties of the flux in the region of thermal neutrons, cross sections given in the JANIS database [39] were used. The neutron self-shielding factors determined by means of numerical simulations with the Monte Carlo N-Particle (MCNP, version 6.1) code [40, 41] were $f_n = 0.813$ for thermal, $f_n = 1.024$ for epithermal and $f_n = 1.010$ for fast neutrons, respectively. These factors were used in the correction for the intereferences arising from (n,γ) reactions.

Gamma rays of neodymium

In total, the measurement of $NdCl_3$ resulted in the identification of 111 prompt gamma rays of neodymium related to inelastic scattering reactions of fast neutrons. These gamma rays are marked in Figs. 1 and 2 and their corresponding data is given in Tables 3, 4, 5, 6, 7, 8, 9 and 10. From all 111

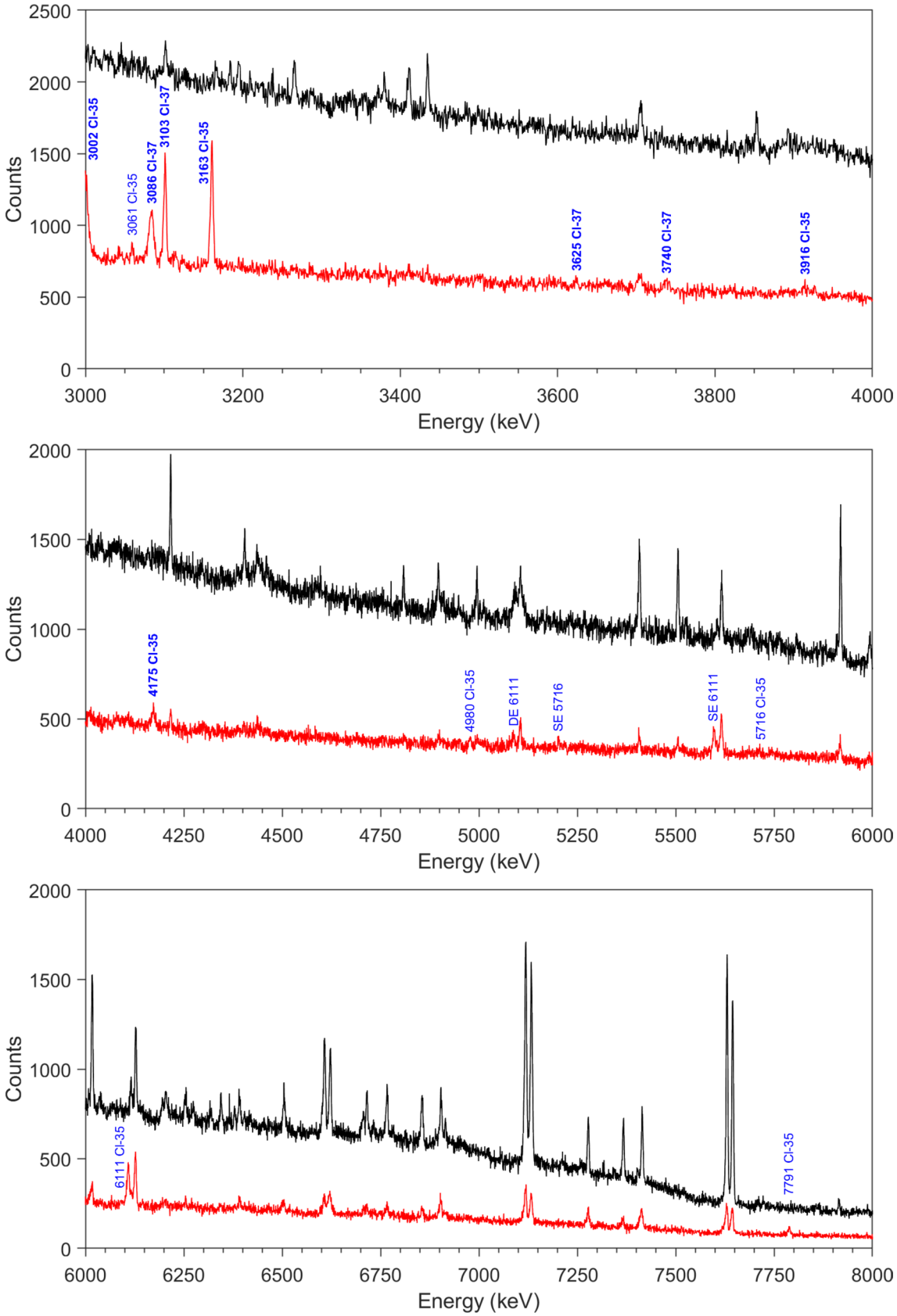
Counts
Energy (keV)
3002 Cl-35
3061 Cl-35
3086 Cl-37
3103 Cl-37
3163 Cl-35
3625 Cl-37
3740 Cl-37
3916 Cl-35
4175 Cl-35
4980 Cl-35
DE 6111
SE 5716
SE 6111
5716 Cl-35
6111 Cl-35
7791 Cl-35

◂**Fig. 2** Measured gamma-ray spectra in the energy range from 3000 to 8000 keV. The spectrum of the $NdCl_3$ sample (red) was obtained during 8886 s counting live time and the spectrum of the beam background (black) during 51,506 s. Prompt gamma rays marked in black and bold are issued from (n,n′γ) inelastic scattering of fast neutrons on neodymium. Gamma rays written in bold blue are induced by inelastic scattering reactions on chlorine. Radiative capture gamma rays from Cl-35 are marked with light blue. Single and double escape peaks are indicated by the abbreviations SE and DE, respectively. Our former publications [9, 18] provide information on the origin of relevant background lines

lines, 14 were associated to ^{142}Nd, 13 to ^{143}Nd, 26 to ^{144}Nd, 7 to ^{145}Nd, 24 to ^{146}Nd, 8 to ^{148}Nd and 11 to ^{150}Nd. Another 8 lines were found to be fed by two isotopes (multi-isotope lines) each with significant contributions (see Table 10). Interferences of lines issued from the ^{35}Cl(n,γ)^{36}Cl, ^{142}Nd(n,γ)^{143}Nd, ^{143}Nd(n,γ)^{144}Nd and ^{145}Nd(n,γ)^{146}Nd reactions were corrected with the intensities derived from [31] and [32], following the method described in [13]. For 45 lines contributions to the net counts were found above 1% and corrected. The contributions for the corresponding lines are given in Table 2. Only several lines of chlorine were Doppler broadened [42, 43]. The composition of the $NdCl_3$ sample was verified from the measurement of the PVC foil performed in our work on $CeCl_3$ [13]. From the interference-free (with respect to data in [20]) chlorine lines at 1185, 1763, 2645, 3002 and 3086 keV (see Figs. 1 and 2) we calculate an average chlorine mass of (0.792 ± 0.004) g, that correponds well with the value derived from the stoichiometry of the sample.

Gamma-ray intensities were determined relative to the 696-keV line of ^{144}Nd. They are presented together with the values determined in [33] in columns 3 and 6 of Tables 3, 4, 5, 6, 7, 8, 9, and 10. We have detected 39 of 44 lines listed in the Demidov Atlas. From the nineteen lines unassigned in [33] we observed the lines at 262.3, 334.2, 582.5, 657.9, 676.6, 748.0, 921.7, 946.6, 971.0, 1149.8, 1162.0, 1247.5 and 1333.1 keV with reasonable counting statistics. With respect to data in [20, 24, 25, 27–29] we found that these lines belong to the (n,n′γ) reactions on neodymium.

For the gamma rays observed in this work at 1671.8 and 2135.1 keV, attributed to the inelastic scattering reactions on ^{144}Nd and ^{143}Nd, respectively, relevant interferences from escape peaks were identified. These lines are interfered by the double escape peak of the 2693.0-keV line of ^{35}Cl and the single escape peak of the 2645.0-keV line of ^{35}Cl. Using the correction curves given in [13], contributions to the net counts of $(20 \pm 4\%)$ and $(54 \pm 5\%)$ were calculated, respectively. For the two lines at 813.7 and 864.0 keV, both associated to the ^{144}Nd(n,n′γ)^{144}Nd reaction, contributions from the single escape peak of the 1323-keV line (^{146}Nd) and of the 1377-keV line ($^{144+146}$Nd) were found to be below 1% and therefore neglected.

The gamma lines listed at energies of 326.4, 439.1, 630.8, 1212.0 and 1446 keV in [33] were all unassigned and not observed in this work. The 326.4-keV line was given with a question mark and the comment "bg?" in [33]. In fact, it is found to be associated to a background line of ^{73}Ge. Data for the lines at 439.1, 630.8 and 1466 keV should be reviewed with caution, since corresponding background lines are given in [33] at 440.0 (^{23}Na), 630.8 (origin unclear) and 1463.3 keV (^{72}Ge). Absence of justified transitions in [20] for the 439.1-keV line could provide support that this line does not belong to neodymium. At energies of 630.8 and 1212.0 keV no relevant line was identified in the measured spectrum, but several transitions could be possible with respect to [20]. In fact, observation of a line around 1466 keV was hindered by the 1463-keV line from the ^{72}Ge(n,n′γ)^{72}Ge reaction produced in the HPGecrystal but might be plausible with regard to data in [20].

We identified 72 new lines with respect to data in [33]. The aforementioned lines are all listed in [20] and from these we assigned 10 to ^{142}Nd, 7 to ^{143}Nd, 18 to ^{144}Nd, 2 to ^{145}Nd, 16 to ^{146}Nd, 8 to ^{148}Nd, 8 to ^{150}Nd. Another 3 lines at 852.4, 1243.3 and 1830.6 keV were found to be fed by two isotopes, ^{145}Nd + ^{150}Nd, ^{145}Nd + ^{146}Nd and ^{144}Nd + ^{146}Nd. In Demidov´s measurement only one single transition of the ^{148}Nd(n,n′γ)^{148}Nd reaction, i.e. the 301.7-keV line [33], was observed. The other lines of ^{148}Nd observed in our measurement were not detected in [33] probably due to their low relative intensities (below 5% in our work) or the impossibility to resolve them from close neighboring lines. The identification of the new lines at 474.0 (^{146}Nd), 527.0 (^{148}Nd), 720.0 (^{150}Nd) and 922.8 keV (^{148}Nd) results from the better energy resolution of our spectrometer, resolving doublets in lines given at energies of 476.6, 525.5, 722.7 and 921.7 keV, respectively, in [33]. The new lines detected at energies of 882.4 and 1333.0 keV, respectively, are assigned to the ^{146}Nd(n,n′γ)^{146}Nd reaction and could not be observed by Demidov owing to close-lying background interferences listed at 880.9 (^{206}Pb) and 1332.6 keV (^{60}Ni) [33]. Observation of the line at 1170.7 keV related to the (n,n′γ) reaction in ^{148}Nd in this work might have been hindered in [33] by a background line listed at 1173.1 keV from ^{60}Ni.

The lines observed in this work at 301.2, 722.0, 946.2, 1249.2 and 1376.6 keV were assigned to two different isotopes of neodymium, i.e. $^{144+148}$Nd, $^{148+150}$Nd, $^{146+148}$Nd, $^{145+148}$Nd and $^{144+146}$Nd, respectively. In Demidov's work the 946.2- and 1249.2-keV lines were unassigned, while the lines at 301.2, 722.0 and 1376.6 keV were associated to ^{148}Nd, ^{150}Nd and ^{146}Nd. In fact, the three aforementioned lines of Demidov et al. were also fed by transitions in ^{144}Nd, ^{144}Nd and ^{148}Nd as further lines at 2073.1, 778.3 and 1022.4 keV from the same levels (2901.4, 2093.3 keV in ^{144}Nd [26], respectively, and 1023.2 keV in ^{148}Nd [29]) were clearly identified.

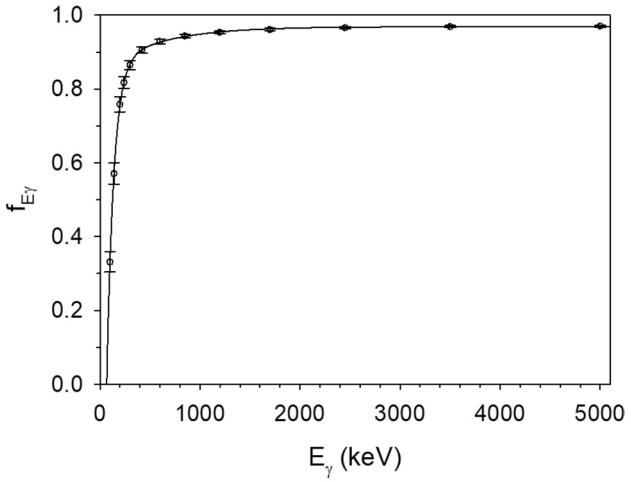

Fig. 3 Variation of the gamma-ray self-absorption factor $f_{E\gamma}$ as a function of the gamma-ray energy E_γ for the measured $NdCl_3$ sample. The data points were obtained from NIST XCOM [34, 35]. The solide line represents the fit of the data with the following relation: $f_{E\gamma} = a_0 + a_1 \cdot \left(1 - e^{-a_2 \cdot E_\gamma}\right) + a_3 \cdot \left(1 - e^{-a_4 \cdot E_\gamma}\right)$ with $a_0 = -\ 1.3968 \pm 0.0443$, $a_1 = 0.1213 \pm 0.0082$, $a_2 = 0.0018 \pm 0.0001$, $a_3 = 2.2442 \pm 0.0384$ and $a_4 = 0.0143 \pm 0.0002$ and E_γ in keV

The line observed at 502.0 keV was not assigned as no plausible transition was identified in [20]. However, it might correspond to a new transition not included in [20] yet, as the counting statistics was acceptable (18.5% uncertainty).

With regard to [31], considerable interferences arising from (n,γ) reactions in ^{142}Nd and ^{143}Nd reactions were expected for the lines observed at 617.4, 696.0, 741.6, 813.7 and 864.0 keV. The intensity ratios relative to Demidov´s work were around one for all these lines except the 741.6- and 813.7-keV lines, for which ratios of 1.87 ± 0.22 and 1.60 ± 0.41 were obtained. These discrepancies might imply either incorrect or missing interference corrections in [33]. Although detailed information for the treatment of (n,γ) interferences is missing in [33], Demidov et al. made use of thermal neutron data listed in [44] (for elements with $Z \leq 46$) and [45] (for elements from $Z = 47$ to $Z = 67$, i.e. Ag to Ho). Absolute gamma-ray intensities of $(34 \pm 1\%)$, $(84 \pm 5\%)$, $(75 \pm 6\%)$, $(12.6 \pm 0.1\%)$ and $(10.8 \pm 0.1\%)$ were derived for the lines mentioned above in order of increasing energy according to data given in [31]. Intensities listed in [45] from private communication with Rasmussen et al. of 23.7, 62, 5.90, 8.87 and 8.82% were found to show significant deviations compared to the values obtained from [31], in particular for the 741.6-keV line. One should be aware that it is unclear if and which of the different data sets listed in [45] were used by Demidov et al. for interference corrections. In addition, the data in [45] seems to be inaccurate compared to the most recent data listed in [31].

The intensities of the gamma lines obtained in this work are plotted against the values listed in [33] in Fig. 4. The average of the intensity ratios, i.e. I_R/I_{RD}, is 1.03 ± 0.34 which indicates a good agreement between the two measurements. To verify the consistency further the residuals R in units of standard deviation [σ] are plotted in the form of a histogram in Fig. 5. The fit of the data with a Gaussian returns an agreement at the 1.5σ level but indicates also a relevant systematic effect as the centroid of the Gaussian is $R = 0.33 \pm 0.12$.

The partial gamma-rays cross sections, averaged over the fast-neutron spectrum are given in column 4 of Tables 3, 4, 5, 6, 7, 8, 9 and 10. For the case of the multi-isotope lines, the partial cross sections were evaluated with the sum of the abundances of the involved isotopes.

E_γ is the gamma-ray energy, $P_{E\gamma}(90°)/(\varepsilon_{E\gamma} \times f_{E\gamma})$ the net counts in the gamma-ray peak divided by the full-energy-peak efficiency and the gamma-ray self-absorption factor, I_R the relative intensity of the gamma-ray and $<\sigma_{E\gamma}(90°)>$ the fission-neutron spectrum-averaged partial cross section for gamma-ray production at an angle of 90° between neutron

Table 1 Effective cross sections $<\sigma>$ for (n,γ) reactions produced from the irradiation of the $NdCl_3$ sample and interfering with (n,n′γ) lines of interest

Neutron-energy range	10^{-10}–1.4×10^{-7} MeV (thermal)			1.4×10^{-7}–0.06 MeV (epithermal)	0.06–20 MeV (fast)
Cross sections	$<\sigma_{th}>$ (b)	$<\sigma_{th}>$ (b)[a]	$<\sigma_{th}>$ (b)[b]	$<\sigma_{epi}>$ (b)	$<\sigma_{fast}>$ (mb)
^{35}Cl(n,γ)^{36}Cl	38(19)	43.61(1)	43.5(4)	0.37(1)	0.72(19)
^{142}Nd(n,γ)^{143}Nd	16.3(79)	18.68(3)	18.7(7)	0.12(2)	23.3(26)
^{143}Nd(n,γ)^{144}Nd	282(137)	323(1)	325(10)	5.01(70)	44(5)
^{145}Nd(n,γ)^{146}Nd	37(18)	44(3)	42(2)	9.14(12)	39(5)
f_n	0.813			1.024	1.010

The $<\sigma>$-values are calculated as described in our previous work [14]. Neutron self-shielding factors f_n for all three neutron-energy ranges considered were determined by means of Monte Carlo simulations with the MCNP6 [40, 41]

[aa]Mean value of cross sections from various data libraries provided in JANIS [39]

[b]: values from [31]

Table 2 Relevant contributions of neutron capture (n,γ) reactions to gamma lines primarily identified as (n,n′γ) lines of neodymium

This work (n,n′γ)		PGNAA database (n,γ)		$P_{E\gamma}(n,\gamma)/P_{E\gamma}$ (%)
E_γ (keV)	^{A}Z	E_γ in keV (^{A}Z)	$I_{E\gamma}$ (%)	
426.0	^{144}Nd	426.7 (^{143}Nd)	1.45 ± 0.06	6.63 ± 1.73
476.2	^{144}Nd	476.8 (^{143}Nd)	4.88 ± 0.20	9.62 ± 2.74
545.2	^{150}Nd	546.8(^{142}Nd)	2.29 ± 0.27	2.84 ± 0.56
588.8	^{146}Nd	589.5 (^{145}Nd)	27.8 ± 1.8	10.1 ± 2.3
617.4	^{144}Nd	618.1 (^{143}Nd)	34 ± 1	9.65 ± 1.85
696.0	^{144}Nd	696.5 (^{143}Nd)	84 ± 6	5.11 ± 0.98
735.4	^{146}Nd	734.4 (^{143}Nd), 735.9 (^{145}Nd)	0.23 ± 0.03 (^{143}Nd), 13.7 ± 0.8 (^{145}Nd)	6.82 ± 2.03
741.6	^{143}Nd	742.1 (^{142}Nd)	75 ± 8	13.8 ± 1.1
778.3	^{144}Nd	778.6 (^{143}Nd)	2.00 ± 0.08	6.52 ± 1.34
813.7	^{144}Nd	814.1 (^{143}Nd)	12.7 ± 1.6	6.49 ± 1.25
864.0	^{144}Nd	863.9 + 864.3 (^{143}Nd)	13.5 ± 0.4	6.42 ± 1.24
936.1	^{148}Nd	936.9 (^{35}Cl)	0.52 ± 0.01	2.76 ± 0.72
979.9	^{144}Nd	980.6 (^{143}Nd)	3.06 ± 0.12	6.91 ± 1.78
1002.3	^{146}Nd	1003.2 (^{143}Nd)	0.35 ± 0.04	1.51 ± 0.33
1006.7	^{142}Nd	1007.3 (^{143}Nd)	0.23 ± 0.02	1.58 ± 0.58
1016.5	^{146}Nd	1016.9 (^{143}Nd), 1017.0 (^{145}Nd)	0.39 ± 0.03 (^{143}Nd), 0.72 ± 0.03 (^{145}Nd)	1.96 ± 0.54
1022.4	^{148}Nd	1023.1 (^{143}Nd)	0.23 ± 0.02	1.41 ± 0.47
1136.7	^{144}Nd	1136.9 (^{143}Nd)	1.78 ± 0.37	13.1 ± 3.6
1161.7	^{145}Nd	1162.7 (^{35}Cl)	2.31 ± 0.09	8.20 ± 2.37
1170.7	^{148}Nd	1170.8 + 1171.8 keV (^{143}Nd), 1170.9 (^{35}Cl)	0.41 ± 0.16 (^{143}Nd), 0.47 ± 0.15 (^{35}Cl)	8.41 ± 3.15
1323.4	^{146}Nd	1323.8 (^{143}Nd), 1323.9 (^{145}Nd)	0.27 ± 0.03 (^{143}Nd), 0.72 ± 0.03 (^{145}Nd)	1.88 ± 0.52
1340.1	^{142}Nd	1340.3 (^{143}Nd)	0.95 ± 0.08 (^{143}Nd)	13.5 ± 3.8
1376.6	^{144}Nd + ^{146}Nd	1376.2 (^{143}Nd)	1.90 ± 0.08 (^{143}Nd)	2.45 ± 0.54
1382.0	^{148}Nd	1383.9 (^{142}Nd)	1.52 ± 0.46 (^{142}Nd)	3.58 ± 0.29
1413.1	^{144}Nd	1413.2 (^{143}Nd)	4.80 ± 0.19 (^{143}Nd)	11.6 ± 3.6
1481.7	^{144}Nd	1482.0 (^{143}Nd)	1.54 ± 0.07 (^{143}Nd)	7.87 ± 1.78
1493.6	^{144}Nd	1493.8 (^{143}Nd)	1.54 ± 0.05 (^{143}Nd)	28.7 ± 11.2
1556.0	^{143}Nd	1555.8 (^{142}Nd)	5.32 ± 0.62 (^{142}Nd)	4.25 ± 0.47
1560.8	^{144}Nd	1560.8 (^{143}Nd)	1.02 ± 0.04 (^{143}Nd)	12.4 ± 3.0
1671.8	^{144}Nd	1671.7 (^{143}Nd)	4.90 ± 0.53 (^{143}Nd)	15.9 ± 3.2
1689.5	^{146}Nd	1690.7 (^{143}Nd)	0.22 ± 0.04 (^{143}Nd)	2.21 ± 0.59
1743.9	^{146}Nd	1743.6 (^{143}Nd)	0.22 ± 0.04 (^{143}Nd)	1.50 ± 0.36
1788.3	^{146}Nd	1787.8 (^{35}Cl)	0.54 ± 0.02 (^{35}Cl)	10.5 ± 3.9
1830.6	^{144}Nd + ^{146}Nd	1828.5 (^{35}Cl), 1831.9 (^{143}Nd)	0.34 ± 0.02 (^{35}Cl), 0.46 ± 0.02 (^{143}Nd)	8.19 ± 2.45
1851.4	^{143}Nd	1852.8 (^{142}Nd)	1.85 ± 0.30	3.57 ± 1.04
1885.0	^{144}Nd	1885.0 (^{143}Nd)	0.22 ± 0.03	3.22 ± 1.51
1894.9	^{144}Nd	1895.7 (^{143}Nd)	0.98 ± 0.034	6.58 ± 1.65
1910.0	^{144}Nd	1909.0 (^{143}Nd)	0.76 ± 0.04	4.70 ± 1.14
1935.5	^{145}Nd	1937.0 (^{35}Cl)	0.46 ± 0.03	7.76 ± 2.40
2022.4	^{144}Nd	2022.1 (^{35}Cl), 2022.5 (^{143}Nd)	0.49 ± 0.02 (^{35}Cl), 0.16 ± 0.02 (^{143}Nd)	12.1 ± 4.1
2035.6	^{143}Nd	2034.6 (^{35}Cl), 2036.1 (^{143}Nd)	0.73 ± 0.02 (^{35}Cl), 0.18 ± 0.01 (^{143}Nd)	15.0 ± 5.8
2073.1	^{144}Nd	2075.4 (^{35}Cl), 2072.7 (^{143}Nd)	0.76 ± 0.02 (^{35}Cl), 0.82 ± 0.03 (^{143}Nd)	8.52 ± 2.97
2135.1	^{143}Nd	2132.3 (^{143}Nd)	0.45 ± 0.02 (^{143}Nd)	3.35 ± 0.69
2185.2	^{144}Nd	2185.6 (^{143}Nd)	0.70 ± 0.03 (^{143}Nd)	2.98 ± 0.63
2845.3	^{142}Nd	2845.5 (^{35}Cl)	1.06 ± 0.01	5.43 ± 1.31

E_γ is the gamma-ray energy, ^{A}Z denotes the considered isotopes, $I_{E\gamma}$ is the absolute gamma-ray intensity and $P_{E\gamma}(n,\gamma)/P_{E\gamma}$ is the fraction of calculated neutron capture counts to the net counts in the gamma line

Table 3 Prompt gamma rays of ^{142}Nd induced by inelastic scattering of fission neutrons

This work				From Demidov Atlas [33]		R
E_γ (keV)	$P_{E\gamma}(90°)/(\varepsilon_{E\gamma} \times f_{E\gamma}) \times 10^{-8}$ (count)	I_R(relative) (%)	$<\sigma_{E\gamma}(90°)>$ (mb)	E_γ (keV)	I_R(relative) (%)	
303.87 ± 0.12	0.18 ± 0.03	1.15 ± 0.17	14.7 ± 2.5	-	-	-
335.79 ± 0.07	0.45 ± 0.04	2.89 ± 0.26	36.9 ± 3.5	334.2 ± 0.3	8.1 ± 1.0	-5.04
502.05 ± 0.19[a]	0.10 ± 0.02	0.66 ± 0.13	-	-	-	-
524.34 ± 0.05	2.32 ± 0.08	14.9 ± 0.7	190 ± 9	525.49 ± 0.10	14.5 ± 1.5[b]	0.62
636.09 ± 0.27	0.11 ± 0.03	0.69 ± 0.20	8.81 ± 2.42	-	-	-
641.41 ± 0.16	0.11 ± 0.03	0.69 ± 0.19	8.81 ± 2.42	-	-	-
875.56 ± 0.11	0.19 ± 0.02	1.21 ± 0.14	15.5 ± 1.7	-	-	-
970.79 ± 0.12[c]	0.19 ± 0.02	1.21 ± 0.15	15.5 ± 1.7	971.0 ± 0.7	2.1 ± 0.5	-1.70
1006.72 ± 0.17[c,d]	0.14 ± 0.03	0.93 ± 0.18	11.9 ± 2.6	-	-	-
1340.09 ± 0.14[d]	0.06 ± 0.01	0.40 ± 0.09	5.11 ± 0.87	-	-	-
1575.61 ± 0.07	7.48 ± 0.29	48 ± 2	613 ± 32	1575.85 ± 0.15	41 ± 4	1.54
2384.14 ± 0.14	0.27 ± 0.02	1.73 ± 0.15	22.1 ± 1.8	-	-	-
2583.26 ± 0.25[c]	0.29 ± 0.03	1.87 ± 0.19	23.9 ± 2.6	-	-	-
2845.33 ± 0.17[e]	0.21 ± 0.02	1.34 ± 0.12	17.1 ± 1.7	-	-	-

E_γ is the gamma-ray energy, $P_{E\gamma}(90°)/(\varepsilon_{E\gamma} \times f_{E\gamma})$ the net counts in the gamma-ray peak divided by the full-energy-peak efficiency and the gamma-ray self-absorption factor, I_R the relative intensity of the gamma-ray and $<\sigma_{E\gamma}(90°)>$ the fission-neutron spectrum-averaged partial cross section for gamma-ray production at an angle of 90° between neutron beam and detector. The residual R is defined in the text by Eq. (2)

[a]Line is attributed to neodymium, but not listed in [20]

[b]524 and 527 keV (doublet not resolved by Demidov)

[c]Corrected for background interference

[d]Corrected for (n,γ) interference from neodymium

[e]Corrected for (n,γ) interference from chlorine

beam and detector. The residual R is defined in the text by Eq. (2)

[a]Corrected for (n,γ) interference from neodymium

[b]Corrected for background interference

[c]474 and 476 keV (doublet not resolved by Demidov)

[d]Corrected for contribution of DE from 2693-keV line of ^{35}Cl (20.1% of net counts)

[e]Corrected for (n,γ) interference from chlorine

Gamma rays of chlorine

The prompt gamma lines of chlorine were also analyzed, and the associated partial cross sections were determined. From all 29 lines observed in the measurement of the $CeCl_3$ reported in [13], the lines at 4111 and 4622 keV from the ^{35}Cl(n,n′γ)^{35}Cl as well as the 4010-keV line from the ^{37}Cl(n,n′γ)^{37}Cl, respectively, were not observed. We assign absence of the aforementioned lines in the $NdCl_3$ spectrum to the detection limit. In addition, data for the lines at 930 (^{35}Cl), 1572 (^{35}S) and 78 keV (^{32}P), respectively, must be reviewed carefully as they contain uncorrected contributions of (n,n′γ) reactions in neodymium with respect to data listed in [20]. Considering the associated uncertainties, the data of both measurements shows an acceptable agreement with each other as shown in Fig. 6. Larger deviations for a few lines could be explained with poor counting statistics.

Detection limit

We define the detection limit (DL) as the smallest quantity of element that produces a net signal above the background over a given counting time. Neutron self-shielding and gamma-ray self-absorption were neglected and the value of the DL calculated from relation (6) given in [16] using the measured beam background and assuming a counting live time of 12 h. The most intense line of neodymium, i.e. the 696-keV line arising primarily from the ^{144}Nd(n,n′γ)^{144}Nd reaction contains a contribution of about 5% produced by radiative capture in ^{143}Nd (see Table 2). Since, for a given neutron-energy spectrum, the interfering capture reaction will always play a relevant role, an effective elemental cross section of $<\sigma^Z_{E\gamma}(90°)> = 354$ mb was determined for this line with an integral neutron flux of $(1.16 \pm 0.04) \times 10^8$ cm^{-2} s^{-1}. Considering a net count uncertainty of 50%, the smallest amount of neodymium that can be detected is 2.1 mg (^{144}Nd, $E_\gamma = 696.0$ keV, $<\sigma^Z_{E\gamma}(90°)> = 354$ mb).

Table 4 Prompt gamma rays of ^{143}Nd induced by inelastic scattering of fission neutrons

This work				From Demidov Atlas [33]		*R*
E_γ (keV)	$P_{E\gamma}(90°)/(\varepsilon_{E\gamma} \times f_{E\gamma}) \times 10^{-8}$ (count)	I_R(relative) (%)	$<\sigma_{E\gamma}(90°)>$ (mb)	E_γ (keV)	I_R(relative) (%)	
580.62 ± 0.19	0.17 ± 0.03	1.07 ± 0.19	30 ± 5	583.5 ± 0.6	1.6 ± 0.3	− 1.52
741.59 ± 0.04[a]	1.55 ± 0.06	9.98 ± 0.51	283 ± 15	742.3 ± 0.3	10 ± 2	− 0.01
1227.95 ± 0.06	0.74 ± 0.05	4.76 ± 0.38	135 ± 10	1228.1 ± 0.4	5.8 ± 0.8	− 1.17
1407.06 ± 0.07[b]	0.75 ± 0.04	4.83 ± 0.28	137 ± 9	1408.0 ± 0.8	6.0 ± 1.5	− 0.77
1431.14 ± 0.08[b]	0.69 ± 0.03	4.47 ± 0.26	127 ± 7	1431.8 ± 0.6	4.9 ± 0.8	− 0.51
1536.06 ± 0.30	0.11 ± 0.02	0.69 ± 0.13	19 ± 4	–	–	–
1556.00 ± 0.10[a,b]	0.33 ± 0.02	2.13 ± 0.16	60 ± 4	1557.0 ± 1.2	2.0 ± 0.5	0.25
1851.40 ± 0.19[a]	0.17 ± 0.02	1.07 ± 0.16	30 ± 4	–	–	–
2011.76 ± 0.32	0.08 ± 0.02	0.54 ± 0.13	15 ± 4	–	–	–
2035.61 ± 0.35[a,b,c]	0.06 ± 0.01	0.38 ± 0.07	11 ± 2	–	–	–
2063.50 ± 0.53	0.11 ± 0.03	0.72 ± 0.17	20 ± 6	–	–	–
2098.61 ± 0.39[b]	0.05 ± 0.01	0.34 ± 0.07	9.6 ± 1.9	–	–	–
2135.15 ± 0.21[a,d]	0.14 ± 0.01	0.87 ± 0.08	25 ± 2	–	–	–

E_γ is the gamma-ray energy, $P_{E\gamma}(90°)/(\varepsilon_{E\gamma} \times f_{E\gamma})$ the net counts in the gamma-ray peak divided by the full-energy-peak efficiency and the gamma-ray self-absorption factor, I_R the relative intensity of the gamma-ray and $<\sigma_{E\gamma}(90°)>$ the fission-neutron spectrum-averaged partial cross section for gamma-ray production at an angle of 90° between neutron beam and detector. The residual *R* is defined in the text by Eq. (2).

[a]Corrected for (n,γ) interference from neodymium

[b]Corrected for background interference

[c]Corrected for (n,γ) interference from chlorine

[d]Corrected for contribution of the single escape peak of the 2645-keV line of ^{35}Cl (54% of net counts)

Conclusion

The emission of prompt gamma rays in neodymium induced by inelastic scattering of fission neutrons in a $NdCl_3$ sample was studied, taken into account relevant interferences from (n,γ) neutron capture lines. Contributions of neutron capture to the net counts of up to about 29% were found.

In total, we identified 111 prompt gamma lines from the (n,n′γ) reactions in neodymium (14 of ^{142}Nd, 13 of ^{143}Nd, 26 of ^{144}Nd, 7 of ^{145}Nd, 24 of ^{146}Nd, 8 of ^{148}Nd, 11 of ^{150}Nd and another 8 related to two isotopes). Another line observed at 502 keV is proposed as a new line associated to fast-neutron inelastic scattering on neodymium, as all other reaction channels were carefully excluded. Relative intensities and fast-neutron spectrum-averaged partial production cross sections of the gamma rays were presented. Compared to the work of Demidov et al. [33] we were able to detect 72 additional lines due to the better energy resolution of our detector and a higher mean neutron-energy. The measured relative intensities are in acceptable agreement with the values provided in [33] (1.5σ level). The detection limit of neodymium was estimated as 2.1 mg for a measuring time of 12 h. Furthermore, the partial gamma-ray production cross sections of the chlorine lines are comparable with the values obtained in [13].

Table 5 Prompt gamma rays of ^{144}Nd induced by inelastic scattering of fission neutrons

This work				From Demidov Atlas [33]		*R*
E_γ (keV)	$P_{E\gamma}(90°)/(\varepsilon_{E\gamma} \times f_{E\gamma}) \times 10^{-8}$ (count)	I_R(relative) (%)	$<\sigma_{E\gamma}(90°)>$ (mb)	E_γ (keV)	I_R(relative) (%)	
426.02 ± 0.16[a]	0.22 ± 0.04	1.42 ± 0.26	21 ± 4	–	–	–
476.15 ± 0.14[a,b]	0.49 ± 0.07	3.16 ± 0.47	46 ± 7	476.6	3.0 ± 1.0[c]	3.27
617.41 ± 0.04[a]	3.14 ± 0.12	20 ± 1	294 ± 15	618.04 ± 0.12	20 ± 3	0.08
695.97 ± 0.04[a]	15.53 ± 0.49	100	1450 ± 68	696.60 ± 0.15	100	–
778.31 ± 0.08[a]	0.29 ± 0.02	1.85 ± 0.16	27 ± 2	778.6 ± 0.6	1.6 ± 0.2	0.97
793.91 ± 0.26	0.08 ± 0.02	0.53 ± 0.13	7.65 ± 1.93	–	–	–
813.68 ± 0.04[a]	1.86 ± 0.07	12.0 ± 0.6	173 ± 9	814.2 ± 0.2	6.4 ± 0.7	6.15
864.01 ± 0.04[a]	1.99 ± 0.07	12.8 ± 0.6	186 ± 9	864.5 ± 0.2	8 ± 2	2.29
979.93 ± 0.09[a,b]	0.41 ± 0.03	2.67 ± 0.18	39 ± 3	980.7 ± 0.5	2.8 ± 0.6	− 0.21
1081.63 ± 0.22	0.06 ± 0.01	0.39 ± 0.09	5.68 ± 0.97	–	–	–
1094.28 ± 0.22	0.18 ± 0.02	1.14 ± 0.15	16.5 ± 1.9	–	–	–
1136.65 ± 0.12[a,b]	0.12 ± 0.01	0.76 ± 0.08	11.1 ± 1.0	–	–	–
1388.42 ± 0.23	0.16 ± 0.02	1.03 ± 0.15	15 ± 2	–	–	–
1413.11 ± 0.08[a,b]	0.37 ± 0.03	2.39 ± 0.19	35 ± 3	1413.3 ± 1.0	2.4 ± 0.8	− 0.02
1451.26 ± 0.18	0.22 ± 0.03	1.43 ± 0.19	21 ± 3	–	–	–
1481.70 ± 0.19[a]	0.18 ± 0.02	1.17 ± 0.15	17 ± 2	–	–	–
1493.55 ± 0.25[a,b]	0.04 ± 0.01	0.25 ± 0.07	3.62 ± 0.91	–	–	–
1560.80 ± 0.14[a]	0.07 ± 0.01	0.47 ± 0.07	6.80 ± 1.00	–	–	–
1671.75 ± 0.12[a,d]	0.21 ± 0.02	1.35 ± 0.11	19.6 ± 2.0	–	–	–
1739.24 ± 0.12	0.28 ± 0.03	1.79 ± 0.18	26 ± 3	–	–	–
1885.01 ± 0.46[a,b]	0.07 ± 0.02	0.44 ± 0.13	6.34 ± 1.82	–	–	–
1894.91 ± 0.24[a]	0.14 ± 0.02	0.91 ± 0.15	13.2 ± 1.9	–	–	–
1910.03 ± 0.23[a]	0.16 ± 0.02	1.00 ± 0.16	14.5 ± 1.9	–	–	–
2022.40 ± 0.39[a,e]	0.05 ± 0.02	0.35 ± 0.11	5.07 ± 2.03	–	–	–
2073.11 ± 0.18[a,b,e]	0.19 ± 0.02	1.20 ± 0.12	17.4 ± 1.9	–	–	-
2185.17 ± 0.23[a]	0.23 ± 0.02	1.50 ± 0.15	22 ± 2	–	–	–

Table 6 Prompt gamma rays of ^{145}Nd induced by inelastic scattering of fission neutrons

This work				From Demidov Atlas [33]		*R*
E_γ (keV)	$P_{E\gamma}(90°)/(\varepsilon_{E\gamma} \times f_{E\gamma}) \times 10^{-8}$ (count)	I_R(relative) (%)	$<\sigma_{E\gamma}(90°)>$ (mb)	E_γ (keV)	I_R(relative) (%)	
657.01 ± 0.04	1.50 ± 0.05	9.68 ± 0.44	402 ± 19	657.9 ± 0.2	12.3 ± 1.3	− 1.91
675.18 ± 0.05	0.42 ± 0.02	2.73 ± 0.16	113 ± 7	676.6 ± 0.4	2.3 ± 0.3	1.26
747.65 ± 0.05[a]	0.58 ± 0.08	3.72 ± 0.55	155 ± 22	748.0 ± 0.5	3.1 ± 0.4	0.91
920.52 ± 0.10[a]	0.31 ± 0.05	2.01 ± 0.32	84 ± 14	921.7 ± 0.4	3.9 ± 0.5[b]	0.16
1161.73 ± 0.14[c]	0.31 ± 0.03	1.97 ± 0.18	82 ± 8	1162.0 ± 1.2	1.6 ± 0.5	0.69
1177.06 ± 0.23[a]	0.09 ± 0.02	0.56 ± 0.14	23 ± 5	–	–	–
1935.52 ± 0.37[c]	0.07 ± 0.02	0.42 ± 0.13	17.5 ± 5.0	–	–	–

E_γ is the gamma-ray energy, $P_{E\gamma}(90°)/(\varepsilon_{E\gamma} \times f_{E\gamma})$ the net counts in the gamma-ray peak divided by the full-energy-peak efficiency and the gamma-ray self-absorption factor, I_R the relative intensity of the gamma-ray and $<\sigma_{E\gamma}(90°)>$ the fission-neutron spectrum-averaged partial cross section for gamma-ray production at an angle of 90° between neutron beam and detector. The residual *R* is defined in the text by Eq. (2)

[a]Corrected for background interference

[b]921 and 923 keV (doublet not resolved by Demidov)

[c]Corrected for (n,γ) interference from chlorine

Table 7 Prompt gamma rays of ^{146}Nd induced by inelastic scattering of fission neutrons

This work				From Demidov Atlas [33]		R
E_γ (keV)	$P_{E\gamma}(90°)/(\varepsilon_{E\gamma} \times f_{E\gamma}) \times 10^{-8}$ (count)	I_R(relative) (%)	$<\sigma_{E\gamma}(90°)>$ (mb)	E_γ (keV)	I_R(relative) (%)	
262.34 ± 0.10	0.25 ± 0.03	1.61 ± 0.19	32 ± 4	262.3 ± 0.6	1.3 ± 0.2	1.12
453.20 ± 0.03	14.44 ± 0.51	93 ± 4	1866 ± 93	453.94 ± 0.10	90 ± 9	0.29
474.00 ± 0.06[a]	0.53 ± 0.05	3.42 ± 0.32	69 ± 7	–	–	–
555.02 ± 0.08	0.32 ± 0.03	2.06 ± 0.18	41 ± 4	–	–	–
588.84 ± 0.03[b]	2.69 ± 0.11	17.3 ± 0.9	348 ± 19	589.69 ± 0.15	16 ± 2	0.61
735.35 ± 0.04[b]	2.06 ± 0.07	13.2 ± 0.6	266 ± 13	736.0 ± 0.3	12 ± 2	0.59
790.43 ± 0.09	0.28 ± 0.02	1.80 ± 0.16	36 ± 3	789.8 ± 0.6	1.8 ± 0.2	0.01
882.40 ± 0.12	0.30 ± 0.03	1.91 ± 0.18	38 ± 4	–	–	–
922.83 ± 0.11[a]	0.31 ± 0.02	1.99 ± 0.17	40 ± 3	–	–	–
1002.27 ± 0.15[b]	0.23 ± 0.03	1.50 ± 0.18	30 ± 4	–	–	–
1016.54 ± 0.08[b]	0.56 ± 0.03	3.61 ± 0.24	73 ± 5	1015.9	5.8 ± 1.0	− 2.13
1149.52 ± 0.09[a]	0.25 ± 0.02	1.64 ± 0.13	33 ± 3	1149.8 ± 1.2	1.4 ± 0.5	0.45
1168.11 ± 0.26	0.15 ± 0.03	0.94 ± 0.19	19 ± 4	–	–	–
1181.78 ± 0.43	0.10 ± 0.02	0.61 ± 0.14	12.3 ± 2.5	–	–	–
1323.38 ± 0.10[b]	0.52 ± 0.03	3.35 ± 0.22	67 ± 4	–	–	–
1332.97 ± 0.11	0.47 ± 0.03	3.03 ± 0.22	61 ± 4	1333.1 ± 0.7	3.1 ± 0.6	–0.10
1470.91 ± 0.08[a]	0.46 ± 0.07	2.95 ± 0.45	59 ± 9	–	–	–
1523.66 ± 0.13	0.30 ± 0.02	1.92 ± 0.17	38 ± 3	–	–	–
1665.65 ± 0.47	0.05 ± 0.02	0.34 ± 0.10	6.79 ± 2.73	–	–	–
1689.51 ± 0.29[b]	0.10 ± 0.02	0.63 ± 0.12	12.6 ± 2.5	–	–	–
1743.95 ± 0.18[b]	0.14 ± 0.02	0.93 ± 0.14	18.7 ± 2.7	–	–	–
1788.29 ± 0.37[c]	0.05 ± 0.02	0.35 ± 0.10	6.97 ± 2.80	–	–	–
1881.47 ± 0.46	0.12 ± 0.03	0.75 ± 0.17	15 ± 4	–	–	–
2119.99 ± 0.48	0.11 ± 0.03	0.69 ± 0.17	14 ± 4	–	–	–

E_γ is the gamma-ray energy, $P_{E\gamma}(90°)/(\varepsilon_{E\gamma} \times f_{E\gamma})$ the net counts in the gamma-ray peak divided by the full-energy-peak efficiency and the gamma-ray self-absorption factor, I_R the relative intensity of the gamma-ray and $<\sigma_{E\gamma}(90°)>$ the fission-neutron spectrum-averaged partial cross section for gamma-ray production at an angle of 90° between neutron beam and detector. The residual R is defined in the text by Eq. (2)

[a]Corrected for background interference

[b]Corrected for (n,γ) interference from neodymium

[c]Corrected for (n,γ) interference from chlorine

Table 8 Prompt gamma rays of ^{148}Nd induced by inelastic scattering of fission neutrons

This work				From Demidov Atlas [33]		*R*
E_γ (keV)	$P_{E\gamma}(90°)/(\varepsilon_{E\gamma} \times f_{E\gamma}) \times 10^{-8}$ (count)	I_R(relative) (%)	$<\sigma_{E\gamma}(90°)>$ (mb)	E_γ (keV)	I_R(relative) (%)	
449.93 ± 0.07	0.68 ± 0.09	4.35 ± 0.61	261 ± 36	–	–	–
489.00 ± 0.13[a]	0.16 ± 0.05	1.03 ± 0.29	62 ± 19	–	–	–
527.03 ± 0.10	0.21 ± 0.03	1.36 ± 0.20	81 ± 12	–	–	–
936.11 ± 0.16[b]	0.22 ± 0.03	1.40 ± 0.18	84 ± 12	–	–	–
1022.42 ± 0.15[a,c]	0.17 ± 0.02	1.07 ± 0.14	64 ± 8	–	–	–
1170.67 ± 0.34[b,c]	0.11 ± 0.02	0.68 ± 0.16	41 ± 7	–	–	–
1382.01 ± 0.28[c]	0.14 ± 0.02	0.87 ± 0.14	52 ± 8	–	–	–
1426.71 ± 0.22	0.15 ± 0.03	0.99 ± 0.17	60 ± 12	–	–	–

E_γ is the gamma-ray energy, $P_{E\gamma}(90°)/(\varepsilon_{E\gamma} \times f_{E\gamma})$ the net counts in the gamma-ray peak divided by the full-energy-peak efficiency and the gamma-ray self-absorption factor, I_R the relative intensity of the gamma-ray and $<\sigma_{E\gamma}(90°)>$ the fission-neutron spectrum-averaged partial cross section for gamma-ray production at an angle of 90° between neutron beam and detector. The residual *R* is defined in the text by Eq. (2)

[a]Corrected for background interference

[b]Corrected for (n,γ) interference from chlorine

[c]Corrected for (n,γ) interference from neodymium

Table 9 Prompt gamma rays of ^{150}Nd induced by inelastic scattering of fission neutrons

This work				From Demidov Atlas [33]		*R*
E_γ (keV)	$P_{E\gamma}(90°)/(\varepsilon_{E\gamma} \times f_{E\gamma}) \times 10^{-8}$ (count)	I_R(relative) (%)	$<\sigma_{E\gamma}(90°)>$ (mb)	E_γ (keV)	I_R(relative) (%)	
130.05 ± 0.03	4.10 ± 0.15	26 ± 1	1615 ± 82	129.97 ± 0.10	42 ± 5	− 3.02
250.87 ± 0.04	1.38 ± 0.05	8.87 ± 0.44	543 ± 27	251.12 ± 0.10	10.1 ± 1.1	− 1.04
338.44 ± 0.16	0.17 ± 0.03	1.11 ± 0.21	68 ± 12	338.4 ± 0.6	2.2 ± 0.5	− 2.01
372.35 ± 0.20	0.29 ± 0.05	1.84 ± 0.34	112 ± 20	–	–	–
545.22 ± 0.08[a]	0.26 ± 0.02	1.67 ± 0.15	102 ± 9	–	–	–
552.47 ± 0.14	0.15 ± 0.02	0.97 ± 0.13	59 ± 8	–	–	–
719.95 ± 0.07	0.50 ± 0.03	3.24 ± 0.21	198 ± 14	–	–	–
755.59 ± 0.14	0.09 ± 0.02	0.59 ± 0.11	36 ± 8	–	–	–
1061.50 ± 0.19	0.17 ± 0.03	1.08 ± 0.22	66 ± 12	–	–	–
1069.90 ± 0.11	0.21 ± 0.02	1.38 ± 0.14	85 ± 9	–	–	–
1124.78 ± 0.13	0.14 ± 0.02	0.91 ± 0.11	56 ± 8	–	–	–

E_γ is the gamma-ray energy, $P_{E\gamma}(90°)/(\varepsilon_{E\gamma} \times f_{E\gamma})$ the net counts in the gamma-ray peak divided by the full-energy-peak efficiency and the gamma-ray self-absorption factor, I_R the relative intensity of the gamma-ray and $<\sigma_{E\gamma}(90°)>$ the fission-neutron spectrum-averaged partial cross section for gamma-ray production at an angle of 90° between neutron beam and detector. The residual *R* is defined in the text by Eq. (2)

[a]Corrected for (n,γ) interference from neodymium

Table 10 Prompt gamma rays of neodymium induced by inelastic scattering of fission neutrons in multiple isotopes

This work					From Demidov Atlas [33]		*R*
E_γ (keV)	^{A}Z	$P_{E\gamma}(90°)/(\varepsilon_{E\gamma} \times f_{E\gamma}) \times 10^{-8}$ (count)	I_R(relative) (%)	$<\sigma_{E\gamma}(90°)>$ (mb)	E_γ (keV)	I_R(relative) (%)	
301.23 ± 0.03	^{144}Nd + ^{148}Nd	4.41 ± 0.14	28 ± 1	332 ± 16	301.71 ± 0.10	37 ± 4	− 2.04
722.01 ± 0.09	^{148}Nd + ^{150}Nd	0.36 ± 0.03	2.34 ± 0.19	71 ± 6	722.7 ± 0.4	4.1 ± 0.5[a]	2.65
852.42 ± 0.18	^{145}Nd + ^{150}Nd	0.28 ± 0.04	1.80 ± 0.29	45 ± 7	–	–	–
946.16 ± 0.12	^{146}Nd + ^{148}Nd	0.23 ± 0.03	1.50 ± 0.17	23 ± 3	946.6 ± 0.8	1.5 ± 0.4	0.00
1243.28 ± 0.16	^{145}Nd + ^{146}Nd	0.12 ± 0.02	0.80 ± 0.14	10.8 ± 1.8	–	–	–
1249.25 ± 0.12	^{145}Nd + ^{148}Nd	0.21 ± 0.02	1.33 ± 0.15	33 ± 3	1247.5	1.5 ± 0.6	− 0.28
1376.56 ± 0.07[b,c]	^{144}Nd + ^{146}Nd	0.76 ± 0.04	4.90 ± 0.28	41 ± 3	1377.2 ± 0.6	4.0 ± 0.6	1.36
1830.60 ± 0.31[b,d]	^{144}Nd + ^{146}Nd	0.10 ± 0.02	0.63 ± 0.12	5.27 ± 1.07	–	–	–

E_γ is the gamma-ray energy, ^{A}Z denotes the contributing isotopes, $P_{E\gamma}(90°)/(\varepsilon_{E\gamma} \times f_{E\gamma})$ the net counts in the gamma-ray peak divided by the full-energy-peak efficiency and the gamma-ray self-absorption factor, I_R the relative intensity of the gamma-ray and $<\sigma_{E\gamma}(90°)>$ the fission-neutron spectrum-averaged partial cross section for gamma-ray production at an angle of 90° between neutron beam and detector. The residual *R* is defined in the text by Eq. (2)

[a]720 and 722 keV (doublet not resolved by Demidov)

[b]Corrected for (n,γ) interference from neodymium

[c]Corrected for background interference

[d]Corrected for (n,γ) interference from chlorine

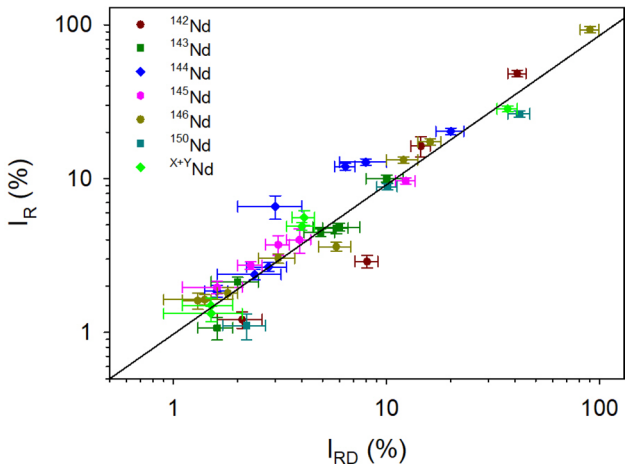

Fig. 4 Correlation between the relative intensities I_R of the prompt gamma rays issued from fission-neutron inelastic scattering (n,n′γ) reactions on neodymium measured in this work and the relative intensities I_{RD} listed in the Demidov Atlas [33]. Data points of $^{X+Y}$Nd indicate multi-isotope lines (see Table 10). The solid line represents the fit of the data with Eq. (1) with a = 0.98 ± 0.10 and b = 0.97 ± 0.05

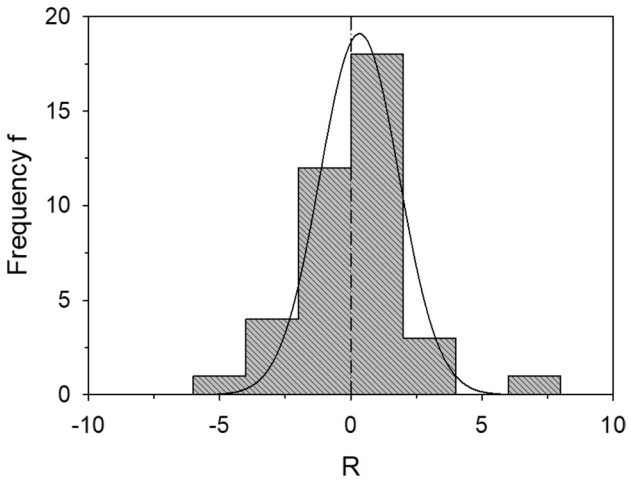

Fig. 5 Histogram plot of the residuals R in units of standard deviation [σ], demonstrating the agreement between the relative intensities of prompt gamma rays induced by inelastic scattering on neodymium derived in this work with the data listed in [33]. The data was fitted with a Gaussian, which is shown by the solid line

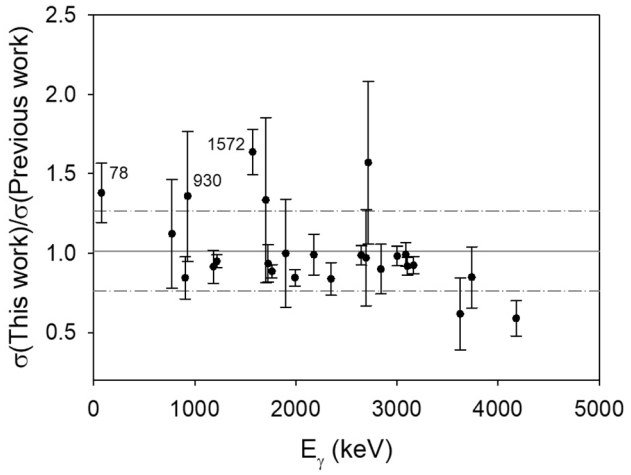

Fig. 6 Ratio of gamma-ray production cross sections $<\sigma_{E\gamma}(90°)>$ in mb for chlorine lines from (n,n′γ) and (n,pγ) reactions obtained in this work compared to these obtained in our previous work [13]. The solid line represents the mean value of the ratios, i.e. 1.01 ± 0.25, while the dash-dotted lines represent the error margins corresponding to one standard deviation

Funding Open Access funding enabled and organized by Projekt DEAL.

Declarations

Competing interests The authors have no competing interests to declare that are relevant to the content of this article. The authors have no affiliations with or involvement in any organization or entity with any financial interest or non-financial interest in the subject matter or materials discussed in this manuscript. Data sets generated during the current study are available from the corresponding author on reasonable request. The 5th author, Zsolt Révay is a member of the Editorial Board of the journal. Therefore, he did not take part in the review process in any capacity and the submission was handled by a different member of the editorial board.

References

1. Molnár GL (2004) Handbook of prompt gamma activation analysis with neutron beams. Kluwer Academic Publishers. ISBN 1-4020-1304-3
2. Schrader CD, Stinner RJ (1961) Remote analysis of surfaces by neutron-gamma-ray inelastic scattering techniques. J Geophys Res 66:1951–1956
3. Jiggins AH, Habbani FI (1976) Prompt gamma-ray analysis using 3.29 MeV neutron inelastic scattering. Int J Appl Raddiat Isot 27:689–693
4. Sowerby BD (1979) Elemental analysis by neutron inelastic scatter gamma rays with a radioisotopeneutron source. Nucl Instrum Methods 166:571–579
5. European Commission. Directorate-General for Internal Market, Industry, Entrepeneurship and SMEs, Blengini GA, EL Latunussa C, Eynard U, Torres de Matos C, Wittmer D, Georgitzikis K, Pavel C, Carrara S, Mancini L, Unguru M, Blagoeva D, Mathieux F, Pennington.(2020) D Study on the EU's list of Critical Raw Materials (2020) Final Report, Publications office, https://data.europa.eu/. https://doi.org/10.2873/11619
6. RMIS—Raw Materials Information System. https://rmis.jrc.ec.europa.eu/eu-critical-raw-materials
7. REGULATION (EU) 2024/1252 OF THE EUROPEAN PARLIAMENT AND OF THE COUNCIL of 11 April 2024 establishing a framework for ensuring a secure and sustainable supply of critical raw materials and amending Regulations (EU) No 168/2013, (EU) 2018/858, (EU) 2018/1724 and (EU) 2019/1020. Official Journal of the European Union. 2024/1252. 3.5.2024. http://data.europa.eu/eli/reg/2024/1252/oj
8. Meleshenkovskii I, Mauerhofer E (2024) Numerical study on the characterization of NdFeB permanent magnets with fast-neutrons induced (n,n'γ) reactions. J Radioanal Nucl Chem 333:2487–2494
9. Ilic Z, Mauerhofer E, Stieghorst C, Révay Zs, Rossbach M, Randriamalala TH, Brückel T (2020) Prompt gamma rays induced by inelastic scattering of fission neutrons on iron. J Radioanal Nucl Chem 325:641–645
10. Mauerhofer E, Ilic Z, Stieghorst C, Révay Zs, Rossbach M, Li J, Randriamalala TH, Brückel T (2021) Prompt and delayed gamma rays induced by epithermal and fast neutrons with indium. J Radioanal Nucl Chem 331:535–546
11. Mauerhofer E, Ilic Z, Stieghorst C, Révay Zs, Vezhlev E, Ophoven N, Randriamalala TH, Brückel T (2022) Prompt gamma rays from fast neutron inelastic scattering on aluminum, titanium and copper. J Radioanal Nucl Chem 331:3987–4000
12. Ophoven N, Ilic Z, Mauerhofer E, Randriamalala TH, Vezhlev E, Stieghorst C, Révay Zs, Brückel T, Jolie J, Strub E (2022) Fast neutron induced gamma rays from (n,n'), (n,p) and (n,α) reactions on CaCO3. J Radioanal Nucl Chem 331:5729–5740
13. Ophoven N, Ilic Z, Mauerhofer E, Randriamalala TH, Vezhlev E, Stieghorst C, Révay Zs, Brückel T, Jolie J, Strub E (2023) Prompt gamma rays from fast neutron induced reactions on cerium and chlorine. J Radioanal Nucl Chem 332:3133–3145
14. Ophoven N, Ilic Z, Mauerhofer E, Randriamalala TH, Vezhlev E, Stieghorst C, Révay Zs, Brückel T, Jolie J, Strub E (2023) Prompt gamma rays of terbium induced by inelastic scattering of fission neutrons. J Radioanal Nucl Chem 333:1287–1300
15. Mauerhofer E, Ophoven N, Ilic Z, Stieghorst C, Révay Zs, Meleshenkovskii I, Randriamalala TH (2024) Gamma emission from interaction of fission neutrons on nickel and zirconium. J Radioanal Nucl Chem 333:4333–4352
16. Ophoven N, Mauerhofer E, Ilic Z, Stieghorst C, Révay Zs, Meleshenkovskii I, Randriamalala TH (2025) Prompt gamma rays of lanthanum and praseodymium produced by inelastic scattering of fission neutrons. J Radioanal Nucl Chem 334:953–967
17. Mauerhofer E, Ophoven N, Ilic Z, Stieghorst C, Révay Zs, Meleshenkovskii I, Randriamalala TH (2025) Prompt gamma rays induced by fission neutrons on sodium, silicon, sulfur and potassium. J Radioanal Nucl Chem. https://doi.org/10.1007/s10967-025-10085-3
18. Randriamalala TH, Rossbach M, Mauerhofer E, Révay Zs, Söllradl S, Wagner FM (2016) FaNGaS: a new instrument for (n,n´γ) reaction measurements at FRM II. Nucl Instrum Methods Phys Res Sect A 806:370–377

19. Révay Zs, Belgya T, Molnár GL (2005) Application of Hypermet-PC in PGAA. J Radioanal Nucl Chem 265:261–265
20. NuDat 3.0 National Nuclear Data Center, Brookhaven National Laboratory https://www.nndc.bnl.gov/nudat3/
21. Chen J, Cameron J, Singh B (2011) Nuclear data sheets for A= 35. Nucl Data Sheets 112:2715–2850
22. Cameron J, Chen J, Singh B, Nica N (2012) Nuclear data sheets for A= 37. Nucl Data Sheets 113:365–514
23. Ouellet C, Singh B (2011) Nuclear data sheets for A= 32. Nucl Data Sheets 112:2199–2355
24. Johnson TD, Symochko D, fadil M, Tuli JK (2011) Nuclear data sheets for A= 142. Nucl Data Sheets 112:1949–2127
25. Tuli JK (1978) Nuclear data sheets for A= 143. Nucl Data Sheets 25:603–673
26. Sonzogni AA (2001) Nuclear data sheets for A= 144. Nucl Data Sheets 93:599–762
27. Browne R, Tuli JK (2009) Nuclear data sheets for A= 145. Nucl Data Sheets 110:507–680
28. Khazov Y, Rodionov A, Shulyak G (2016) Nuclear data sheets for A= 146. Nucl Data Sheets 136:163–452
29. Nica N (2014) Nuclear data sheets for A= 148. Nucl Data Sheets 117:1–229
30. Basu SK (2013) Nuclear data sheets for A= 150. Nucl Data Sheets 114:435–660
31. Révay Zs, Firestone RB, Belgya T, Molnár (2004) Prompt gamma-ray spectrum. In: Molnár GL (ed) Handbook of prompt gamma activation analysis with neutron beams. Kluwer Academic Publishers, Dordrecht, pp 173–364
32. Database for Prompt Gamma-ray Neutron Activation Analysis, International Atomic Energy Agency Nuclear Data Services https://www-nds.iaea.org/pgaa/
33. Demidov A, Govor L, Cherepantsev M, Ahmed S, Al-Najjar M, Al-Amili N, Al-Assafi N, Rammo N (1978) Atlas of Gamma-Ray Spectra from the Inelastic Scattering of Reactor Fast Neutrons. Atomizdat, Moscow
34. NIST XCOM: Photons Cross Sections Database, National Institute of Standards and Technology https://physics.nist.gov/PhysRefData/Xcom/html/xcom1.html
35. Berger MJ, Hubbell JH, Seltzer S, Chang J, Coursey JS, Sukumar R, Zucker DS (2009) XCOM: photon cross sections database. NIST Stand Ref Database 8:87–3597
36. Brown DA et al (2018) ENDF/B-VIII.0: the 8th major release of the nuclear reaction data library with CIELO-project cross sections, new standards and thermal scattering data. Nucl Data Sheets 148:1–142
37. MacFarlane RE, Kahler AC (2010) Methods for processing ENDF/B-VII with NJOY. Nucl Data Sheets 111:2739–2890
38. MacFarlane R, Muir DW, Boicourt RM, Kahler AC, Conlin JL (2017) The NJOY Nuclear Data Processing System, Version 2016. https://doi.org/10.2172/1338791
39. OECD NEA Data Bank, (2020) JANIS Book of neutron-induced cross-sections https://www.oecd-nea.org/janis/book/book-neutron-2020-09.pdf
40. Initial MCNP6 Release Overview MCNP6 Version 1.0, Los Alamos National Laboratory report LA-UR-13-22934
41. Goorley T et al (2017) Initial MCNP6 release overview. Nucl Technol 180:298–315
42. Barzilov A, Womble P (2014) Study of doppler broadening of gamma-ray spectra in 14-MeV neutron activation analysis. J Radioanal Nucl Chem 301:811–819
43. Catz AL, Amiel S (1967) Study of lifetimes of nuclear levels by Doppler broadening attenuation using a (Ge)Li gamma-ray spectrometer. Nucl Phys A 92:222–232
44. Bartholomew GA, Doveika A, Eastwood KM, Monaro S, Groshev LV, Demidov AM, Pelekhov VI, Sokolovskii LL (1967) Compendium of thermal-neutron-capture γ-ray measurements part I Z≤46. Nucl Data Sheets 3:367–650
45. Groshev LV, Demidov AM, Pelekhov VI, Sokolovskii LL, Bartholomew GA, Doveika A, Eastwood KM, Monaro S (1968) Compendium of thermal-neutron-capture γ-ray measurements part II Z= 47 to Z= 67 (Ag to Ho). Nucl Data Sheets 5:1–242